




# Physicochemical Improvement of Carvacrol Loaded Nanostructured Lipid Carrier (NLC)

Rachmat Mauludin<sup>1,\*</sup> , Afrillia N. Garmana<sup>2</sup> , Fikri Fauzian<sup>1</sup> 

<sup>1</sup> Department of Pharmaceutics, School of Pharmacy, Institut Teknologi Bandung, Bandung 40132, Indonesia

<sup>2</sup> Department of Pharmacology and Clinical Pharmacy, School of Pharmacy, Institut Teknologi Bandung, Bandung 40132, Indonesia

\* Correspondence: [rachmat@fa.itb.ac.id](mailto:rachmat@fa.itb.ac.id) (R.M.);

Scopus Author ID 25959283200

Received: 1.02.2024; Accepted: 12.05.2024; Published: 21.07.2024

**Abstract:** Carvacrol (CAR) is a compound widely used in pharmaceuticals. However, CAR exhibits low solubility in water. Nanostructured lipid carrier (NLC) can improve the physicochemical properties of CAR. This research aims to optimize and characterize the CAR-loaded NLC. The CAR-NLC formulation was optimized using the Box-Behnken design. The CAR concentration, surfactant concentration, and homogenization time are the independent variables. Particle size, encapsulation efficiency, and drug loading are the dependent variables. The Box-Behnken design optimized the CAR-NLC by demonstrating particle size, encapsulation efficiency, and drug loading of 174.5 nm, 98.46 %, and 42.20 %, respectively. The optimum CAR-NLC characterization showed a zeta potential of -24.83 mV, a round or oval particle shape, and exhibited an endothermic event at the range of 48.62 to 53.16°C. The CAR-NLC formulations are expected to be an alternative in improving the physicochemical properties of CAR for future applications.

**Keywords:** Box-Behnken design; carvacrol; characterization; formulation; nanostructured lipid carrier.

© 2024 by the authors. This article is an open-access article distributed under the terms and conditions of the Creative Commons Attribution (CC BY) license (<https://creativecommons.org/licenses/by/4.0/>).

## 1. Introduction

In recent years, there has been a significant increase in the use of natural products for various applications in the pharmaceutical, food, and cosmetic fields. Natural products are considered to be a safer and more affordable option than synthetic compounds. Research on natural products such as medicinal plants and their derivative compounds provides benefits to society in increasing their applications and benefits [1-7]. Carvacrol (CAR) is a phenolic monoterpene compound contained within essential oils derived from oregano (*Origanum vulgare* L.), thyme (*Thymus vulgaris* L.), black cumin (*Nigella sativa* L.), and marjoram (*Origanum majorana* L.). CAR is categorized as a generally recognized safe (GRAS) compound and is widely used in pharmaceutical, food, and cosmetic applications. CAR has biological activities such as antioxidant, antibacterial, antifungal, anti-inflammatory, analgesic, anticancer, hepatoprotective, spasmolytic, and vasorelaxant. CAR is also widely used in food and cosmetics as a flavoring, preservative, and fragrance [8-11]. However, the benefits possessed by CAR face challenges in its application due to its low solubility in water, strong odor, rapid oxidation, and volatilization [12-14].

Encapsulation of hydrophobic and unstable compounds into nanotechnology-based drug delivery systems is one of the available strategies to improve their physicochemical

properties. Among the various nanotechnology-based drug delivery systems, nanostructured lipid carrier (NLC) provides several advantages, such as being biodegradable, biocompatible, low toxicity, being able to keep active substances from degradation, and providing controlled release of active substances [15,16]. NLC is the latest generation of lipid nanoparticles, which consist of a mixture of solid and liquid lipids dispersed in a surfactant solution. By adding liquid lipids to the formula, NLC is able to increase the loading capacity of active substances in the system and prevent the release of active substances during storage compared to solid lipid nanoparticles (SLN), whose formula only consists of solid lipids [17-19].

Therefore, this study aims to formulate CAR in the NLC system (which shall be referred to as CAR-NLC in this study) and optimize the formula by applying the Box-Behnken experimental design with the independent variables: CAR concentration, surfactant concentration, and homogenization time to measure the responses to particle size, encapsulation efficiency, and drug loading. Statistical experimental design has been widely used to optimize formulations more efficiently, such as the response surface methodology (RSM), which can produce equations that describe the surface response as a polynomial function of the experimental variables. A number of studies have succeeded in optimizing the NLC formula using the Box-Behnken design by requiring a smaller number of experiments to understand its correlation and significance between the independent and dependent variables [20,21]. Zeta potential value, morphology, thermal characteristics, and stability will further characterize the optimum CAR-NLC formula.

## 2. Materials and Methods

### 2.1. Materials.

Carvacrol (CAR) with  $\geq 98.5\%$  purity was obtained from Shanghai Macklin Biochemical Co., Ltd. (Shanghai, China). Tween<sup>®</sup> 80 was obtained from Merck Co. (Darmstadt, Germany). TEGO<sup>®</sup> Care 165 was obtained from Evonik Co. (Essen, Germany). Beeswax (BW) was obtained from RAS Chemical (Bandung, Indonesia). Analytical grade water (Onelab Waterone<sup>™</sup>) was obtained from PT. Jayamas Medica Industry (Sidoarjo, Indonesia). Analytical-grade ethanol was obtained from PT. Smart Lab Indonesia (Tangerang Selatan, Indonesia). The other reagents used in the study were of analytical grade.

### 2.2. Preparation of CAR-NLC.

The preparation for the CAR-NLC formula was conducted using the hot homogenization-ultrasonication method. The lipid phase consists of CAR, TEGO<sup>®</sup> Care 165, and beeswax (BW) (in a fixed ratio of 3.5%, w/v), while the aqueous phase consists of Tween<sup>®</sup> 80 and Onelab Waterone<sup>™</sup>. The TEGO<sup>®</sup> Care 165 and Tween<sup>®</sup> 80 surfactant ratio was 1:4. The lipid and aqueous phases were prepared separately; they were heated until reaching a temperature of  $70 \pm 2^\circ\text{C}$  for 10 minutes. While maintaining a similar temperature, the aqueous phase was then gradually poured into the lipid phase while being homogenized using the high-shear homogenizer (Ultra-Turrax<sup>®</sup> T-25, IKA-Works, Inc., Staufen im Breisgau, Germany) at 7,000 rpm for a certain period. Consecutively, the probe-type ultrasonicator (CY-500 Ultrasonic Homogenizer, J.P. Selecta, Barcelona, Spain) was employed to reduce the particle size further. The particle size reduction process was performed at a 70% amplitude setting for a period of 7 minutes and a pulse cycle of 45 seconds on and 15 seconds off. This process was conducted inside an ice bath to maintain a low temperature and prevent temperature increase,

which may disrupt the CAR-NLC formula. The obtained NLC formula was then allowed to reach room temperature. The total volume of the NLC formula obtained was 20 mL.

### 2.3. Optimization of CAR-NLC formula using Box-Behnken experiment design.

The independent variables were chosen to optimize the CAR-NLC formulation by applying the Box-Behnken experimental design: CAR concentration ( $X_1$ ), surfactant concentration ( $X_2$ ), and homogenization time ( $X_3$ ). Each variable exhibited three observed levels: low (-1), medium (0), and high (+1). The dependent variables, or responses, were particle size (PS) ( $Y_1$ ), encapsulation efficiency (EE) ( $Y_2$ ), and drug loading (DL) ( $Y_2$ ). The values and objectives of each variable are shown in Table 1. The Box-Behnken experimental design was applied to produce a polynomial function of the independent variables toward response and predict the area in which the independent variables produce an optimal response. As many as 15 formulas of CAR-NLC were composed according to the compositions made with the software Minitab<sup>®</sup> WEB (Minitab, Inc., State College, PA, USA) as shown in Table 2, and the polynomial function was made according to the experimental design following the Equation 1.

$$Y_i = \beta_0 + \beta_1 X_1 X_1 + \beta_2 X_2 + \beta_3 X_3 + \beta_{11} X_1 X_1 + \beta_{22} X_2 X_2 + \beta_{33} X_3 X_3 + \beta_{12} X_1 X_2 + \beta_{13} X_1 X_3 + \beta_{23} X_2 X_3$$

Equation 1

$Y_i$  is the estimated response related to each combination of independent variable levels,  $\beta_0$  is the intercept, and  $\beta_1$  to  $\beta_{33}$  are the coefficients measured from the experimental value of  $Y_i$ . The analysis of variance (ANOVA) was also applied to determine the significance of the model, and a  $P$ -value lower than 0.05 indicates a statistically significant model.

### 2.4. Particle size, polydispersity index, and zeta potential measurement.

The dynamic light scattering (DLS) method was used to analyze the particle size of the formulation, and the photon correlation spectroscopy (Delsa<sup>™</sup> Nano C Particle Analyzer, Beckman Coulter, Brea, CA, USA) was employed. The particle size distribution was then illustrated with polydispersity index (PDI). The same instrument was also used to determine the zeta potential value but with the electrophoretic light-scattering (ELS) method. For the determination of particle size and PDI, the sample was diluted 20 times with Onelab Waterone<sup>™</sup>, put into disposable semi-micro cuvettes, and measured. For the zeta potential analysis, the sample was diluted 200 times with Onelab Waterone<sup>™</sup>, then put into a flat surface cell and analyzed.

### 2.5. Encapsulation efficiency and drug loading measurement.

CAR's encapsulation efficiency (EE) and drug loading (DL) within the NLC formula were measured using an indirect method. First, the CAR-NLC formula was centrifuged for 30 minutes using the centrifugal ultrafilter device (10 kDa, Amicon Ultra, Millipore, Billerica, MA, USA) at 13,000 rpm speed. The filtrate was then collected and redissolved in ethanol to determine the amount of unencapsulated CAR, which was measured with a UV-visible spectrophotometer (DU 7500i, Beckman Coulter, Brea, CA, USA) at the wavelength 275 nm. The amount of CAR within the solution was determined using the calibration curve of CAR in ethanol at the concentration range of 15-55  $\mu\text{g/mL}$  [4]. Equation 2 and Equation 3 below were used to determine the value of EE and DL, respectively.

$$EE (\%) = \frac{\text{the total amount of CAR} - \text{the amount of free CAR}}{\text{the total amount of CAR}} \times 100 \quad \text{Equation 2}$$

$$DL (\%) = \frac{\text{the total amount of CAR} - \text{the amount of free CAR}}{\text{amount of BW}} \times 100 \quad \text{Equation 3}$$

### 2.6. Morphology analysis.

The morphology of the CAR-NLC particle was analyzed using transmission electron microscopy (TEM) (HT7700, Hitachi, Tokyo, Japan) at 100 kV. A drop of the optimum CAR-NLC formula was put onto a carbon-coated copper grid with a mesh size of 200 nm to perform the morphology analysis. A negative staining process was then carried out with the UranylLess EM Stain by applying 15  $\mu$ L of the staining agent onto the grid and letting it sit for 1 minute before commencing the analysis.

### 2.7. Thermal characteristic analysis.

The thermal characteristic of the samples was analyzed using differential scanning calorimetry (DSC) (DSC-60 Plus, Shimadzu, Kyoto, Japan). Prior to the thermal analysis, the NLC was centrifuged at 13,000 rpm for 30 minutes using a centrifugal ultrafilter device (10 kDa MWCO, Amicon Ultra, Millipore, Billerica, MA, USA) to reduce the water content. As much as 2-8 mg of BW, TEGO<sup>®</sup> Care 165, concentrate of the Blank-NLC (optimum NLC formula without CAR addition), and concentrate of the optimum CAR-NLC formula were put into a closed aluminum pan and heated at the temperature range of 30-90°C with a heating rate of 10°C/minutes and nitrogen purge of 50 mL/minutes. An empty aluminum pan was used as a reference.

### 2.8. Stability study.

The stability study of the optimum CAR-NLC formula was performed at temperatures 4, 25, and 40°C for 84 days. Samples were collected at the 0, 14, 28, 42, 56, 70, and 84-day time stamps to be further analyzed in regards to their particle size (PS) and its polydispersity index (PDI). The encapsulation efficiency (EE) of the optimum CAR-NLC formula was also carried out to evaluate the probability of CAR being released from the NLC during storage.

### 2.9. Statistical analysis.

The statistical analysis and data visualization was performed by using the software Minitab<sup>®</sup> WEB (Minitab, Inc., State College, PA, USA) and GraphPad Prism v.8.0 (InStat 3.06, San Diego, CA, USA). One-way ANOVA was used to determine the statistical significance of the difference. The difference is statistically significant if the *P*-value < 0.05.

## 3. Results and Discussion

### 3.1. CAR-NLC formula optimization.

The CAR-NLC formula was constructed from the beeswax (BW) solid lipid and a combination of Tween<sup>®</sup> 80 and TEGO<sup>®</sup> Care 165 surfactants according to the performed simple excipient screening results. BW was chosen as the solid lipid component for the CAR-NLC formulation because the simple binary mixture of CAR 30% and BW (w/w) were able to combine and solidify back with the mixture melting point above 40°C [15,16]. Other solid lipids such as stearic acid, cetyl alcohol, and stearyl alcohol, which also underwent the

screening process, did not yield similar results. Meanwhile, the combination of Tween® 80 and TEGO® Care 165 surfactants was chosen because the combination of said surfactants was able to form the CAR-NLC formula with the lowest particle size and polydispersity index (PDI) compared to the single Tween® 80 formula, or the combination of Tween® 80 and Poloxamer 188, or Tween® 80 and propylene glycol.

The CAR-NLC formula was optimized using the Box-Behnken design. Three independent variables with the most influence toward the CAR-NLC formula characteristic were chosen according to the preliminary study using factorial design, consisting of CAR concentration ( $X_1$ ), surfactant concentration ( $X_2$ ), and homogenization time ( $X_3$ ), while the analyzed response of this optimization is the particle size (PS) ( $Y_1$ ), encapsulation efficiency (EE) ( $Y_2$ ), and drug loading (DL) ( $Y_3$ ) as shown in Table 1. Table 2 displayed 15 tested formulas for the CAR-NLC formula optimization step along with the obtained response. Every CAR-NLC formula exhibited a PDI value of less than 0.5, demonstrating the uniform CAR-NLC particle size distribution [22].

**Table 1.** Independent and dependent variables in Box-Behnken design.

Independent variables	Levels		
	Low (-1)	Medium (0)	High (+1)
$X_1$ : CAR concentration (% w/v)	0.5	1.0	1.5
$X_2$ : surfactant concentration (% w/v)	6.0	6.5	7.0
$X_3$ : homogenization time (min)	6.0	7.0	8.0
Dependent variables	Goal		
$Y_1$ : particle size (nm)	Minimize		
$Y_2$ : encapsulation efficiency (%)	Maximize		
$Y_3$ : drug loading (%)	Maximize		

**Table 2.** Experimental design and observed responses of Box–Behnken design.

Run	Independent variables			Observed responses			PDI
	$X_1$	$X_2$	$X_3$	$Y_1$	$Y_2$	$Y_3$	
1	0.5	6.5	6	225.3	96.14	13.73	0.25
2	0.5	6.5	8	306.2	96.63	13.80	0.35
3	1.5	6.0	7	199.2	98.20	42.08	0.44
4	0.5	6.0	7	249.5	94.38	13.48	0.37
5	1.0	7.0	6	240.5	97.92	27.98	0.26
6	1.0	6.0	6	277.7	97.50	27.86	0.29
7	1.5	6.5	8	176.0	98.78	42.33	0.33
8	1.0	7.0	8	200.5	97.79	27.94	0.38
9	1.5	7.0	7	171.7	97.78	41.90	0.42
10	1.0	6.5	7	190.7	96.66	27.62	0.26
11	0.5	7.0	7	208.5	96.99	13.86	0.42
12	1.0	6.5	7	198.1	96.55	27.58	0.27
13	1.0	6.0	8	277.2	98.43	28.12	0.33
14	1.0	6.5	7	199.1	96.50	27.57	0.27
15	1.5	6.5	6	277.6	98.16	42.07	0.36

$X_1$ : CAR concentration (% w/v),  $X_2$ : surfactant concentration (% w/v),  $X_3$ : homogenization time (min),  $Y_1$ : particle size (nm),  $Y_2$ : encapsulation efficiency (%),  $Y_3$ : drug loading (%), PDI: polydispersity index.

Three polynomial equations were created using the Box-Behnken design to analyze the relationship between the independent variable and response and predict the area of the independent variable, which yielded the optimum response. Table 3 shows each regression model's calculated correlation coefficient value ( $R^2$ ). All models showed an  $R^2$  value above 0.800, proving that the results of the experiments were similar to those of the constructed statistical model, thus proving it to be the best model to be chosen [23-25].



**Table 3.** ANOVA results were obtained for the regression model.

Parameter	Y <sub>1</sub> (PS)		Y <sub>2</sub> (EE)		Y <sub>3</sub> (DL)	
	Coefficient	P-value	Coefficient	P-value	Coefficient	P-value
Intercept	2590	0.000	156.4	0.000	22	0.000
X <sub>1</sub>	476	0.001	22.3	0.001	30.4	0.000
X <sub>2</sub>	-284	0.001	-12.3	0.137	-4.40	0.447
X <sub>3</sub>	-432.4	0.051	-9.89	0.147	-2.81	0.023
X <sub>1</sub> X <sub>1</sub>	17.1	0.377	-0.43	0.622	0.50	0.011
X <sub>2</sub> X <sub>2</sub>	27.9	0.175	1.50	0.127	0.47	0.014
X <sub>3</sub> X <sub>3</sub>	46	0.000	0.97	0.005	0.27	0.000
X <sub>1</sub> X <sub>2</sub>	13.5	0.462	-3.03	0.012	-0.56	0.005
X <sub>1</sub> X <sub>3</sub>	-91.3	0.000	0.07	0.875	0.10	0.174
X <sub>2</sub> X <sub>3</sub>	-19.8	0.067	-0.53	0.236	-0.15	0.054
R <sup>2</sup>	0.986		0.957		0.999	

X<sub>1</sub>: CAR concentration, X<sub>2</sub>: surfactant concentration, X<sub>3</sub>: homogenization time, Y<sub>1</sub>: particle size (PS), Y<sub>2</sub>: encapsulation efficiency (EE), Y<sub>3</sub>: drug loading (DL), R<sup>2</sup>: R-squared (correlation coefficient).

### 3.1.1. Effect of independent variables on particle size (Y<sub>1</sub>).

The polynomial equation demonstrating the relationship between the independent variable (X<sub>i</sub>) and the response Y<sub>1</sub> (particle size) is shown in Equation 4.

$$Y_1 = 2590 + 476X_1 - 284X_2 - 432.4X_3 + 17.1X_1X_1 + 27.9X_2X_2 + 463X_3 + 13.5X_1X_2 - 91.3X_1X_3 - 19.8X_2X_3$$

Equation 4

The obtained CAR-NLC particle size varied from 171.1 to 306.2 nm (refer to Table 2). The ANOVA analysis shown in Table 3 revealed that the variables X<sub>1</sub> (CAR concentration) and X<sub>2</sub> (surfactant concentration) significantly affect the CAR-NLC particle size (*P*-value < 0.05), while the effect of the variable X<sub>3</sub> (homogenization time) was insignificant towards the CAR-NLC particle size (*P*-value > 0.05). CAR not only acts as the active substance, but it also serves as the liquid lipid in the NLC formulation. The contour plot figure (Figure 1A) also shows that the increase in CAR concentration would decrease the CAR-NLC particle size. The reason was that the increase of CAR concentration in the formula might decrease the viscosity of the formula's internal phase, causing the lipid globules to be dispersed more easily during the hot homogenization process and the further CAR-NLC particle size reduction during the ultrasonication process [26]. Figure 1A also shows that the increase in surfactant concentration will decrease the CAR-NLC particle size. The reason behind this was that surfactant was able to decrease the interface tension of the aqueous and lipid phases, causing the formation of smaller lipid globules during the hot homogenization process. The high surfactant concentration at a certain limit may stabilize the nanoparticle by forming steric hindrance, which prevents nanoparticle aggregation [27,28].

### 3.1.2. Effect of independent variables on encapsulation efficiency (Y<sub>2</sub>).

The polynomial equation demonstrating the relationship between the independent variable (X<sub>i</sub>) and the response Y<sub>2</sub> (encapsulation efficiency) is shown in Equation 5.

$$Y_2 = 156.4 + 22.3X_1 - 12.3X_2 - 9.89X_3 - 0.43X_1X_1 + 1.50X_2X_2 + 0.97X_3X_3 - 3.03X_1X_2 + 0.07X_1X_3 - 0.53X_2X_3$$

Equation 5

The CAR-NLC encapsulation efficiency varied from 94.38 to 98.78% (refer to Table 2). The ANOVA analysis shown in Table 3 revealed that the variable X<sub>1</sub> (CAR concentration) significantly affects the CAR-NLC encapsulation efficiency (*P*-value < 0.05), while the effect of the variables X<sub>2</sub> (surfactant concentration) and X<sub>3</sub> (homogenization time) were insignificant

toward the CAR-NLC encapsulation efficiency ( $P$ -value > 0.05). On the contour plot figure (Figure 1B), it is also shown that the increase in CAR concentration will increase the encapsulation efficiency of CAR-NLC. This may happen due to the decrease of the CAR-NLC particle size as the CAR concentration increases. Smaller-sized nanoparticles possess a larger surface area to volume ratio, rendering them able to encapsulate more active substances [29,30]. This may happen due to the effect of CAR redistribution from the aqueous phase toward the lipid phase during the hot homogenization process, which is continued by a temperature decrease. The mixture of lipid and aqueous phases at high temperatures caused the increase of CAR solubility in the aqueous phase, and CAR distribution from the lipid phase toward the aqueous phase occurred. After the homogenization process is finished, the lipid globules and aqueous phase will decrease temperature, and the globule lipid core will start to crystallize with the relatively larger amount of CAR within the aqueous phase. Further temperature decrease renders the CAR to undergo the supersaturated condition because the solubility of CAR decreases within the aqueous phase, and CAR will attempt to return to the lipid phase (redistribution process). The solid lipid core has formed, and CAR will continue to accumulate in the liquid outer region [31]. The smaller lipid globules' size during the hot homogenization due to the increase of CAR concentration (where the surface area to volume ratio is larger), then the redistribution and accumulation of CAR from the aqueous phase toward the globule surface is more efficient, thus improving the encapsulation process. The important aspect is that the CAR concentration increase would increase the CAR-NLC encapsulation efficiency, but only until the limit at which the CAR concentration increase yielded negative results [32], which did not occur in this study.

### 3.1.3. Effect of independent variables on drug loading ( $Y_3$ ).

The polynomial equation demonstrating the relationship between the independent variable ( $X_i$ ) and the response  $Y_3$  (drug loading) is shown in Equation 6.

$$Y_3 = 22 + 30.4X_1 - 4.40X_2 - 2.81X_3 + 0.50X_1X_1 + 0.47X_2X_2 + 0.27X_3X_3 - 0.56X_1X_2 + 0.10X_1X_3 - 0.15X_2X_3$$

Equation 6

The CAR-NLC drug loading varied from 13.48 to 42.33% (refer to Table 2). According to the ANOVA analysis shown in Table 3, it revealed that the variables  $X_1$  (CAR concentration) and  $X_3$  (homogenization time) significantly affect the CAR-NLC drug loading ( $P$ -value < 0.05). In contrast, the variable  $X_2$  (surfactant concentration) was insignificant toward the CAR-NLC drug loading ( $P$ -value > 0.05). CAR is the lipid-soluble active ingredient; therefore, the CAR-NLC drug loading was directly proportional to its encapsulation efficiency [18]. On the contour plot figure (Figure 1C), it is also shown that the increase in CAR concentration will also increase the CAR-NLC drug loading. As shown in Table 2, the 15 tested formulas of CAR-NLC exhibited a high encapsulation efficiency (>90%). Most of the CAR was trapped within the NLC matrix, either the CAR with low (0.5%, w/v), medium (1.0%, w/v), or high (1.5%, w/v) concentration. According to Equation 6, the drug loading will increase when the BW solid lipid concentration is constant while the CAR concentrations increase. The homogenization time also significantly affects the CAR drug loading into the NLC matrix due to the CAR redistribution from the aqueous phase towards the lipid globules for the encapsulation process, which happened during the hot homogenization process, continued by the temperature decline, as elaborated before [31].

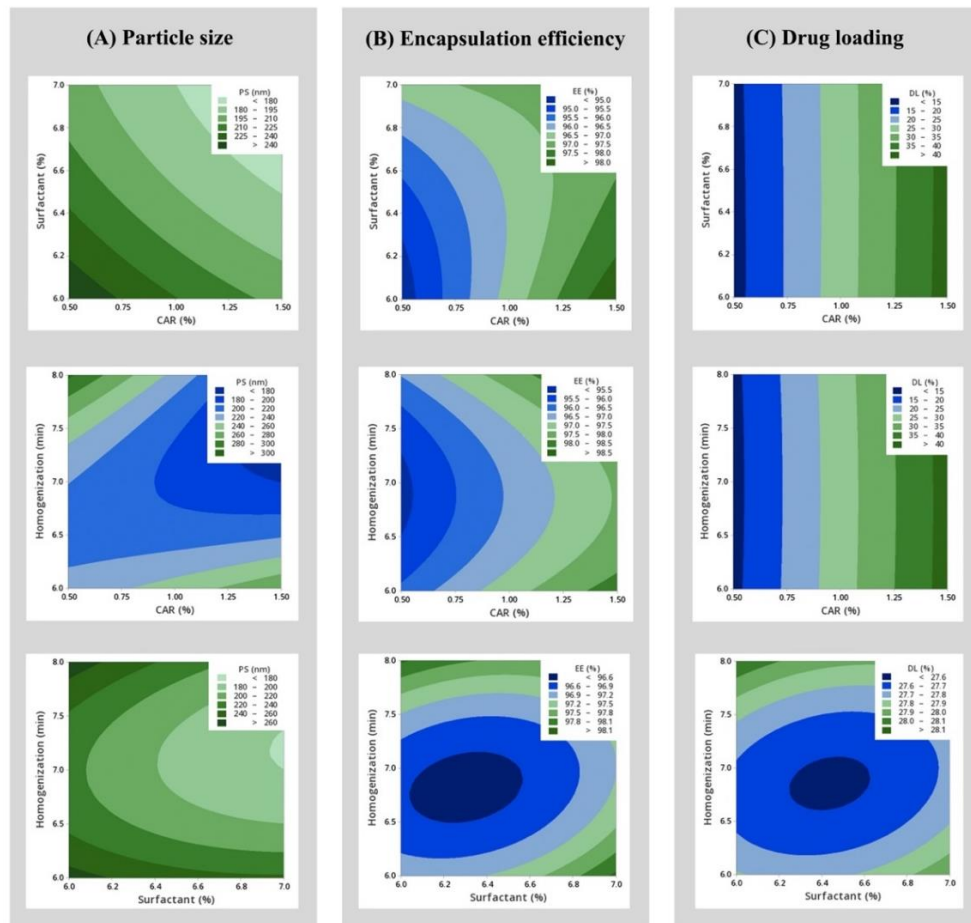


**Figure 1.** Contour plots for the effect of CAR concentration (% w/v), surfactant concentration (% w/v), and homogenization time (min) on (A) particle size (PS) (nm); (B) encapsulation efficiency (EE) (%); (C) drug loading (DL) (%) of the CAR-NLC formula generated using Box-Behnken design.

### 3.1.4. Selection of optimum CAR-NLC formula.

The optimum CAR-NLC formula was chosen according to the criteria listed in Table 1: exhibiting minimum particle size, maximum encapsulation efficiency, and maximum drug loading. The formula was chosen with the assistance of the response optimizer tool from the software Minitab® WEB (Minitab, Inc., State College, PA, USA).

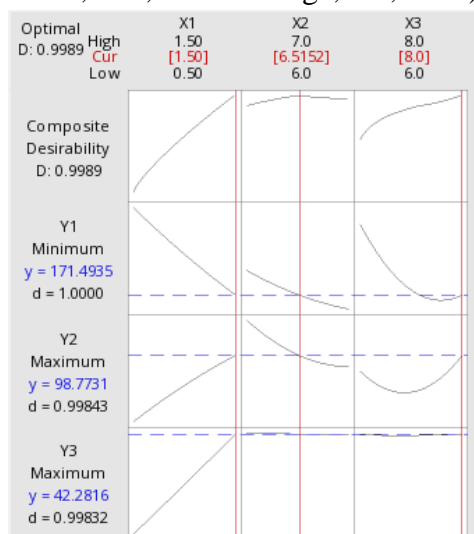


**Figure 2.** Optimization plots of the responses Y<sub>1</sub>: particle size (nm), Y<sub>2</sub>: encapsulation efficiency (%), and Y<sub>3</sub>: drug loading (%) based on independent variables X<sub>1</sub>: CAR concentration (% w/v), X<sub>2</sub>: surfactant concentration (% w/v), and X<sub>3</sub>: homogenization time (min) generated using Box-Behnken design.



According to the optimization plots (refer to Figure 2), the optimum value for the independent variables  $X_1$ ,  $X_2$ , and  $X_3$  was 1.5% (w/v) CAR, 6.5% (w/v) surfactant, and 8 minutes of homogenization time, respectively. The independent variables were predicted to produce the response  $Y_1$  (PS),  $Y_2$  (EE), and  $Y_3$  (DL) as much as 171.5 nm, 98.77%, and 42.28%, respectively. The desirability value for total and individual responses was found to equate to one (1); therefore, this optimized formula had a high chance of obtaining similar values experimentally [20].

### 3.1.5. Confirmation of optimum CAR-NLC formula.

The CAR-NLC was produced with the optimum formula, and the result was compared with the predicted values from the Box-Behnken design, as shown in Table 4. The experimental values obtained for the responses  $Y_1$  (PS),  $Y_2$  (EE), and  $Y_3$  (DL) were  $174.5 \pm 1.2$  nm,  $98.46 \pm 0.07\%$ , and  $42.20 \pm 0.03\%$ , respectively. It revealed that the error percentage obtained from the three responses was relatively low (below 5%), confirming that the Box-Behnken design model has successfully optimized the CAR-NLC formula. The optimum CAR-NLC formula exhibited PDI and zeta potential values of  $0.31 \pm 0.04$  and  $-24.83 \pm 5.51$  mV, respectively. The PDI parameter showed that the particle size distribution of CAR-NLC was uniform, without any aggregation between particles occurring. At the same time, the zeta potential parameter showed that the CAR-NLC exhibited improved stability in its liquid phase [33].

**Table 4.** Comparison of the predicted and observed values from the optimized formula of Box-Behnken design.

Response	Predicted value	Observed value	Error (%)
$Y_1$ : particle size (nm)	171.5	$174.5 \pm 1.2$	1.75
$Y_2$ : encapsulation efficiency (%)	98.77	$98.46 \pm 0.07$	0.32
$Y_3$ : drug loading (%)	42.28	$42.20 \pm 0.03$	0.19

Error (%) =  $(|\text{predicted value} - \text{observed value}| / \text{predicted value}) \times 100$ . Data were expressed as mean  $\pm$  standard deviation (n=3).

### 3.2. Morphology analysis.

The morphology analysis for the optimum CAR-NLC formula was carried out by using transmission electron microscopy (TEM). Figure 3 shows that the optimum CAR-NLC formula exhibited spherical or oval-shaped particles, with diameters ranging from 160-200 nm, which was in accordance with the particle size data of the DLS instrument analysis. The TEM image also showed no aggregation between the particles.

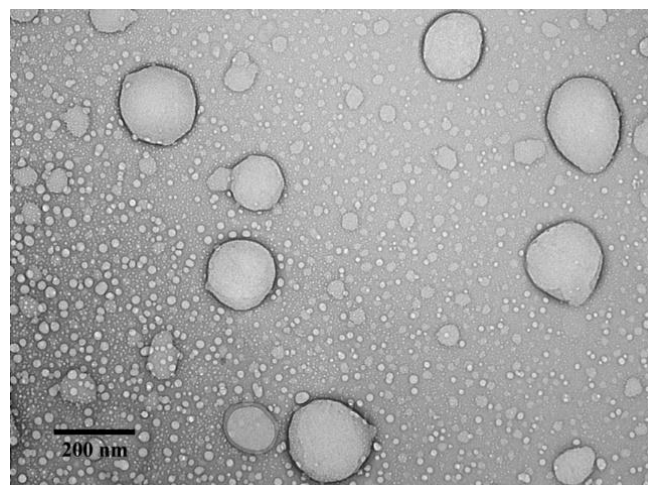


**Figure 3.** TEM image showing the morphology of the optimum CAR-NLC formula.

### 3.3. Thermal characteristic analysis.

Differentiating scanning calorimetry (DSC) is an instrument used to characterize the NLC formula and its constituents. The DSC thermogram provides information regarding a substance's physical characteristics and crystallinity according to its thermal profile [34].

The DSC thermograms of BW solid lipid (a), TEGO<sup>®</sup> Care 165 surfactant (b), Blank-NLC (c), and optimum CAR-NLC formula (d) are shown in Figure 4. The BW solid lipid DSC thermogram exhibited an endothermic event in the range of 40.85 to 48.49°C ( $T_{\text{peak}} = 45.45^{\circ}\text{C}$ ), which correlated to its melting point. The TEGO<sup>®</sup> Care 165 DSC thermogram exhibited two endothermic peaks in the range of 44.33 to 55.53°C ( $T_{\text{peak1}} = 46.85^{\circ}\text{C}$  and  $T_{\text{peak2}} = 54.03^{\circ}\text{C}$ ). This wide range of melting points was caused by the solid lipid structure composed of glyceryl stearate and PEG-100 stearate [35,36]. TEGO<sup>®</sup> Care 165 is a self-emulsifying lipid that acts not only as an emulsifier but also as a lipid solidification agent [34,35].

The DSC thermogram of the Blank-NLC exhibited an endothermic event in the range of 50.33 to 53.96°C ( $T_{\text{mid}} = 52.15^{\circ}\text{C}$ ), characterizing its glass transition temperature ( $T_g$ ). Glass transition is a reversible transition that occurs toward amorphous materials heated or cooled down in a certain temperature range. During the temperature decrease, the material becomes brittle (less flexible), resembling glass, and if heat is applied, the material becomes rubbery [37]. The glass transition is characterized by a thermal profile resembling a staircase, starting from its baseline from its DSC thermogram. Usually, the occurring deviation was relatively small if the sample was a single organic material (such as lipid) without being dispersed in a carrier. However, the Blank-NLC sample was dispersed in water, which is why a relatively large deviation was observed, caused by the water's large heat capacity [38]. The DSC thermogram of the optimum CAR-NLC formula exhibited an endothermic event at the range 48.62 to 53.16°C ( $T_{\text{peak}} = 51.22^{\circ}\text{C}$ ), and no glass transition was observed. This may be caused by the CAR addition (lipophilic liquid matter), which acts as a plasticizer, lowering the brittleness of the NLC matrix and rendering it more flexible [39,40].

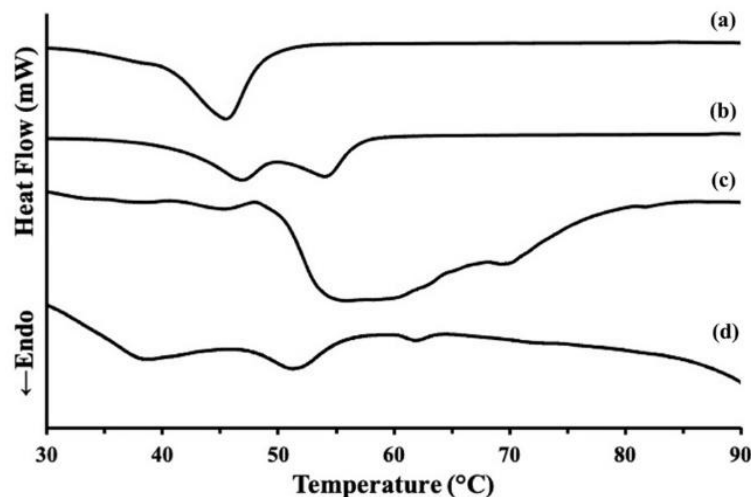


**Figure 4.** DSC thermograms of (a) beeswax; (b) TEGO<sup>®</sup> Care 165; (c) Blank-NLC; (d) CAR-NLC.

### 3.4. Stability study.

The stability study evaluates the optimum CAR-NLC formula by the following parameters: particle size (PS), polydispersity index (PDI), and encapsulation efficiency (EE) for 84 days at the storage temperature of 4, 25, and 40°C; the result was provided at Figure 5. It can be observed that the optimum CAR-NLC formula did not undergo a significant increase

in particle size ( $P$ -value  $> 0.05$ ) at day 84 ( $197.3 \pm 17.5$  nm) compared to the initial value at day 0 ( $174.5 \pm 1.2$  nm) when stored at  $4^{\circ}\text{C}$ . However, when stored at 25 and  $40^{\circ}\text{C}$ , there was a significant increase in particle size ( $P$ -value  $< 0.05$ ). The CAR-NLC storage at  $25^{\circ}\text{C}$  exhibited particle size increase starting at day 56 ( $196.6 \pm 11.0$  nm), while at  $40^{\circ}\text{C}$  the particle size increase starting on day 28 ( $193.1 \pm 11.0$  nm), compared to the initial value. On day 84, the optimum CAR-NLC formula stored at 25 and  $40^{\circ}\text{C}$  exhibited particle size increases as much as  $210.0 \pm 10.5$  nm and  $228.6 \pm 7.5$  nm, respectively. For the PDI and EE parameters, the optimum CAR-NLC formula did not change significantly at day 84 compared to day 0 for all storage conditions (4, 25, and  $40^{\circ}\text{C}$ ). The PDI value obtained from every observation point and storage condition was less than 0.5. This PDI value indicates a uniform CAR-NLC particle size distribution [22,41-43]. The EE value obtained from every observation point and storage condition was also within the 98-99% range, indicating that CAR stayed within the NLC matrix during the storage period.

Therefore, it revealed that the optimum CAR-NLC formula was stable for 84 days at  $4^{\circ}\text{C}$ . Meanwhile, at 25 and  $40^{\circ}\text{C}$ , the optimum CAR-NLC formula exhibited an increase in particle size without any CAR release from the NLC matrix, which can be caused by aggregation between the NLC particles. Strong electrostatic force and low system kinetic energy at low temperatures may provide excellent stability toward the formula. The instability of the NLC formula stored at higher temperatures might be due to the high system kinetic energy, leading to a higher chance for collision and aggression between particles, as explained by Shu *et al.* (2023) in their stability study of lutein-loaded NLC [44].

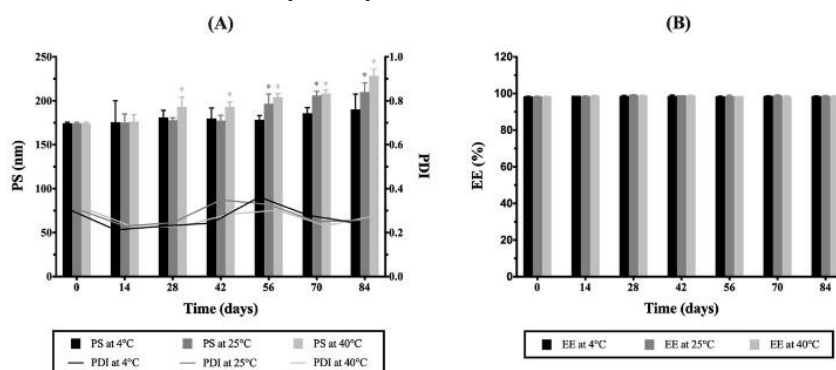


**Figure 5.** Evaluation of NLC stability regarding their (A) particle size (PS) and polydispersity index (PDI); (B) encapsulation efficiency (EE) along 84 days. Data were expressed as mean  $\pm$  standard deviation ( $n = 3$ ). \* $P$ -value  $< 0.05$  was considered significant compared to the data day 0.

#### 4. Conclusions

In this study, CAR has been successfully formulated into the NLC drug delivery system to improve its physicochemical properties. The CAR-NLC formula was made using the hot homogenization-ultrasonication method by applying the Box-Behnken experimental design for the optimization process. The optimum CAR-NLC formula is composed of 1.5% (w/v) CAR as the active substance, 3.5% (w/v) BW as the solid lipid, and a combination surfactant of TEGO<sup>®</sup> Care 165 and Tween<sup>®</sup> 80 (1:4) 6.5% (w/v) which can produce the optimum NLC formula with particle size, encapsulation efficiency, and drug loading of  $174.5 \pm 1.2$  nm (with a PDI of  $0.31 \pm 0.04$ ),  $98.46 \pm 0.07\%$ , and  $42.20 \pm 0.03\%$ , respectively. The optimum CAR-NLC formula was further characterized, and the result showed the zeta potential value of  $-24.83 \pm 5.51$  mV, with a round or oval particle shape based on TEM analysis; it also showed

an endothermic event at the range of 48.62 to 53.16°C ( $T_{\text{peak}} = 51.22^{\circ}\text{C}$ ) based on DSC analysis, and finally, the formula was stable for 84 days at 4°C.

## Funding

The research was supported by the Directorate General of Higher Education, Research, and Technology, Ministry of Education, Culture, Research, and Technology, the Republic of Indonesia, through the Master's Thesis Research grant scheme year 2022 (Grant number: 083/E5/PG.02.00.PT/2022).

## Acknowledgments

The authors would like to thank The School of Pharmacy ITB and the Directorate General of Higher Education, Research, and Technology, Ministry of Education, Culture, Research, and Technology, the Republic of Indonesia.

## Conflicts of Interest

The authors declare no conflict of interest.

## References

1. Kazemi, M.; Mohammadifar, M.; Aghadavoud, E.; Vakili, Z.; Aarabi, M.H.; Talaei, S.A. Deep skin wound healing potential of lavender essential oil and licorice extract in a nanoemulsion form: Biochemical, histopathological and gene expression evidences. *J. Tissue Viability* **2020**, *29*, 116–124, <https://doi.org/10.1016/j.jtv.2020.03.004>.
2. Qadir, A.; Jahan, S.; Aqil, M.; Warsi, M.H.; Alhakamy, N.A.; Alfaleh, M.A.; Khan, N.; Ali, A. Phytochemical-Based Nano-Pharmacotherapeutics for Management of Burn Wound Healing. *Gels* **2021**, *7*, 209, <https://doi.org/10.3390/gels7040209>.
3. Nasim, N.; Sandeep, I.S.; Mohanty, S. Plant-derived natural products for drug discovery: current approaches and prospects. *The Nucleus* **2022**, *65*, 399–411, <https://doi.org/10.1007/s13237-022-00405-3>.
4. Atanasov, A.G.; Zotchev, S.B.; Dirsch, V.M.; Orhan, I.E.; Banach, M.; Rollinger, J.M.; Barreca, D.; Weckwerth, W.; Bauer, R.; Bayer, E.A.; Majeed, M.; Bishayee, A.; Bochkov, V.; Bonn, G.K.; Braid, N.; Bucar, F.; Cifuentes, A.; D'Onofrio, G.; Bodkin, M.; Diederich, M.; Dinkova-Kostova, A.T.; Efferth, T.; El Bairy, K.; Arkells, N.; Fan, T.-P.; Fiebich, B.L.; Freissmuth, M.; Georgiev, M.I.; Gibbons, S.; Godfrey, K.M.; Gruber, C.W.; Heer, J.; Huber, L.A.; Ibanez, E.; Kijjoo, A.; Kiss, A.K.; Lu, A.; Macias, F.A.; Miller, M.J.S.; Mocan, A.; Müller, R.; Nicoletti, F.; Perry, G.; Pittalà, V.; Rastrelli, L.; Ristow, M.; Russo, G.L.; Silva, A.S.; Schuster, D.; Sheridan, H.; Skalicka-Woźniak, K.; Skaltsounis, L.; Sobarzo-Sánchez, E.; Bredt, D.S.; Stuppner, H.; Sureda, A.; Tzvetkov, N.T.; Vacca, R.A.; Aggarwal, B.B.; Battino, M.; Giampieri, F.; Wink, M.; Wolfender, J.-L.; Xiao, J.; Yeung, A.W.K.; Lizard, G.; Popp, M.A.; Heinrich, M.; Berindan-Neagoe, I.; Stadler, M.; Daglia, M.; Verpoorte, R.; Supuran, C.T.; the International Natural Product Sciences, T. Natural products in drug discovery: advances and opportunities. *Nat. Rev. Drug Discov.* **2021**, *20*, 200–216, <https://doi.org/10.1038/s41573-020-00114-z>.
5. Ribeiro, G.d.J.G.; Rei Yan, S.L.; Palmisano, G.; Wrenger, C. Plant Extracts as a Source of Natural Products with Potential Antimalarial Effects: An Update from 2018 to 2022. *Pharmaceutics* **2023**, *15*, 1638, <https://doi.org/10.3390/pharmaceutics15061638>.
6. Fauzian, F.; Garmana, A.N.; Mauludin, R. Applications of Nanotechnology-Based Drug Delivery System for Delivering Natural Products into Acute and Chronic Wounds: A Review. *Biointerface Res. Appl. Chem.* **2023**, *13*, 426, <https://doi.org/10.33263/BRIAC135.426>.
7. Hariyanti, H.; Mauludin, R.; Sumirtapura, Y.C.; Kurniati, N.F. A Review: Pharmacological Activities of Quinoline Alkaloid of *Cinchona* sp. *Biointerface Res. Appl. Chem.* **2023**, *13*, 319, <https://doi.org/10.33263/BRIAC134.319>.
8. Laothaweerungsawat, N.; Neimkhum, W.; Anuchapreeda, S.; Sirithunyulug, J.; Chaiyana, W. Transdermal delivery enhancement of carvacrol from *Origanum vulgare* L. essential oil by microemulsion. *Int. J. Pharm.*



- 2020, 579, 119052, <https://doi.org/10.1016/j.ijpharm.2020.119052>.
9. Santos, E.H.; Kamimura, J.A.; Hill, L.E.; Gomes, C.L. Characterization of carvacrol beta-cyclodextrin inclusion complexes as delivery systems for antibacterial and antioxidant applications. *LWT - Food Sci. Technol.* **2015**, *60*, 583–592, <https://doi.org/10.1016/j.lwt.2014.08.046>.
  10. Sharifi-Rad, M.; Varoni, E.M.; Iriti, M.; Martorell, M.; Setzer, W.N.; del Mar Contreras, M.; Salehi, B.; Soltani-Nejad, A.; Rajabi, S.; Tajbakhsh, M.; Sharifi-Rad, J. Carvacrol and human health: A comprehensive review. *Phytother. Res.* **2018**, *32*, 1675-1687, <https://doi.org/10.1002/ptr.6103>.
  11. Imran, M.; Aslam, M.; Alsagaby, S.A.; Saeed, F.; Ahmad, I.; Afzaal, M.; Arshad, M.U.; Abdelgawad, M.A.; El-Ghorab, A.H.; Khames, A.; Shariati, M.A.; Ahmad, A.; Hussain, M.; Imran, A.; Islam, S. Therapeutic application of carvacrol: A comprehensive review. *Food Sci Nutr.* **2022**, *10*, 3544–3561, <https://doi.org/10.1002/fsn3.2994>.
  12. He, J.; Huang, S.; Sun, X.; Han, L.; Chang, C.; Zhang, W.; Zhong, Q. Carvacrol Loaded Solid Lipid Nanoparticles of Propylene Glycol Monopalmitate and Glyceryl Monostearate: Preparation, Characterization, and Synergistic Antimicrobial Activity. *Nanomaterials* **2019**, *9*, 1162, <https://doi.org/10.3390/nano9081162>.
  13. Mączka, W.; Twardawska, M.; Grabarczyk, M.; Wińska, K. Carvacrol—A Natural Phenolic Compound with Antimicrobial Properties. *Antibiotics* **2023**, *12*, 824, <https://doi.org/10.3390/antibiotics12050824>.
  14. Khan, S.; Sharma, A.; Jain, V. An Overview of Nanostructured Lipid Carriers and its Application in Drug Delivery through Different Routes. *Adv. Pharm. Bull.* **2023**, *13*, 446-460, <https://doi.org/10.34172/apb.2023.056>.
  15. Galvão, J.G.; Santos, R.L.; Lira, A.A.M.; Kaminski, R.; Sarmiento, V.H.; Severino, P.; Dolabella, S.S.; Scher, R.; Souto, E.B.; Nunes, R.S. Stearic Acid, Beeswax and Carnauba Wax as Green Raw Materials for the Loading of Carvacrol into Nanostructured Lipid Carriers. *Appl. Sci.* **2020**, *10*, 6267, <https://doi.org/10.3390/APP10186267>.
  16. Attama, A.A.; Müller-Goymann, C.C. Effect of beeswax modification on the lipid matrix and solid lipid nanoparticle crystallinity. *Colloids Surf. A: Physicochem. Eng. Asp.* **2008**, *315*, 189-195, <https://doi.org/10.1016/j.colsurfa.2007.07.035>.
  17. Haider, M.; Abdin, S.M.; Kamal, L.; Orive, G. Nanostructured Lipid Carriers for Delivery of Chemotherapeutics: A Review. *Pharmaceutics* **2020**, *12*, 288, <https://doi.org/10.3390/pharmaceutics12030288>.
  18. Muller, H.R.; Shegokar, R.; M. Keck, C. 20 Years of Lipid Nanoparticles (SLN & NLC): Present State of Development & Industrial Applications. *Curr. Drug Discov. Technol.* **2011**, *8*, 207–227, <https://doi.org/10.2174/157016311796799062>.
  19. Tamjidi, F.; Shahedi, M.; Varshosaz, J.; Nasirpour, A. Nanostructured lipid carriers (NLC): A potential delivery system for bioactive food molecules. *Innov. Food Sci. Emerg. Technol.* **2013**, *19*, 29–43, <https://doi.org/10.1016/j.ifset.2013.03.002>.
  20. Kim, M.-H.; Kim, K.-T.; Sohn, S.-Y.; Lee, J.-Y.; Lee, C.H.; Yang, H.; Lee, B.K.; Lee, K.W.; Kim, D.-D. Formulation and evaluation of nanostructured lipid carriers (NLCs) of 20 (S)-protopanaxadiol (PPD) by Box-Behnken design. *Int. J. Nanomedicine* **2019**, *14*, 8509–8520, <https://doi.org/10.2147/IJN.S215835>.
  21. Aslam, M.; Aqil, M.; Ahad, A.; Najmi, A.K.; Sultana, Y.; Ali, A. Application of Box–Behnken design for preparation of glibenclamide loaded lipid based nanoparticles: Optimization, *in vitro* skin permeation, drug release and *in vivo* pharmacokinetic study. *J. Mol. Liq.* **2016**, *219*, 897-908, <https://doi.org/10.1016/j.molliq.2016.03.069>.
  22. Mura, P.; Maestrelli, F.; D’Ambrosio, M.; Luceri, C.; Cirri, M. Evaluation and Comparison of Solid Lipid Nanoparticles (SLNs) and Nanostructured Lipid Carriers (NLCs) as Vectors to Develop Hydrochlorothiazide Effective and Safe Pediatric Oral Liquid Formulations. *Pharmaceutics* **2021**, *13*, 437, <https://doi.org/10.3390/pharmaceutics13040437>.
  23. Son, G.-H.; Na, Y.-G.; Huh, H.W.; Wang, M.; Kim, M.-K.; Han, M.-G.; Byeon, J.-J.; Lee, H.-K.; Cho, C.-W. Systemic Design and Evaluation of Ticagrelor-Loaded Nanostructured Lipid Carriers for Enhancing Bioavailability and Antiplatelet Activity. *Pharmaceutics* **2019**, *11*, 222, <https://doi.org/10.3390/pharmaceutics11050222>.
  24. Vilcapoma, W.; de Bruijn, J.; Elías-Peñañiel, C.; Espinoza, C.; Farfán-Rodríguez, L.; López, J.; Encina-Zelada, C.R. Optimization of Ultrasound-Assisted Extraction of Dietary Fiber from Yellow Dragon Fruit Peels and Its Application in Low-Fat Alpaca-Based Sausages. *Foods* **2023**, *12*, 2945, <https://doi.org/10.3390/foods12152945>.



25. Chin, S.-F.; Jong, S.-J.; Yeo, Y.-J. Optimization of Cellulose-Based Hydrogel Synthesis Using Response Surface Methodology. *Biointerface Res. Appl. Chem.* **2022**, *12*, 7136-7146, <https://doi.org/10.33263/BRIAC126.71367146>.
26. Kraisit, P.; Sarisuta, N. Development of Triamcinolone Acetonide-Loaded Nanostructured Lipid Carriers (NLCs) for Buccal Drug Delivery Using the Box-Behnken Design. *Molecules* **2018**, *23*, 982, <https://doi.org/10.3390/molecules23040982>.
27. Harshita; Barkat, M.A.; Rizwanullah, M.; Beg, S.; Pottoo, F.H.; Siddiqui, S.; Ahmad, F.J. Paclitaxel-loaded Nanolipidic Carriers with Improved Oral Bioavailability and Anticancer Activity against Human Liver Carcinoma. *AAPS PharmSciTech* **2019**, *20*, 87, <https://doi.org/10.1208/s12249-019-1304-4>.
28. Soni, K.; Rizwanullah, M.; Kohli, K. Development and optimization of sulforaphane-loaded nanostructured lipid carriers by the Box-Behnken design for improved oral efficacy against cancer: *in vitro*, *ex vivo* and *in vivo* assessments. *Artif. Cells Nanomed. Biotechnol.* **2018**, *46*, 15–31, <https://doi.org/10.1080/21691401.2017.1408124>.
29. Ezhilarasu, H.; Vishalli, D.; Dheen, S.T.; Bay, B.-H.; Srinivasan, D.K. Nanoparticle-Based Therapeutic Approach for Diabetic Wound Healing. *Nanomaterials* **2020**, *10*, 1234, <https://doi.org/10.3390/nano10061234>.
30. Singh, R.; Lillard Jr, J.W. Nanoparticle-based targeted drug delivery. *Exp. Mol. Pathol.* **2009**, *86*, 215-223, <https://doi.org/10.1016/j.yexmp.2008.12.004>.
31. Müller, R.H.; Radtke, M.; Wissing, S.A. Solid lipid nanoparticles (SLN) and nanostructured lipid carriers (NLC) in cosmetic and dermatological preparations. *Adv. Drug Deliv. Rev.* **2002**, *54*, S131–S155, [https://doi.org/10.1016/S0169-409X\(02\)00118-7](https://doi.org/10.1016/S0169-409X(02)00118-7).
32. Suciati, T.; Nafisa, S.; Nareswari, T.L.; Juniatic, M.; Julianti, E.; Wibowo, M.S.; Yudhistira, T.; Ihsanawati, I.; Triyani, Y.; Khairurrijal, K. ArtinM Grafted Phospholipid Nanoparticles for Enhancing Antibiotic Cellular Uptake Against Intracellular Infection. *Int. J. Nanomedicine* **2020**, *15*, 8829–8843, <https://doi.org/10.2147/IJN.S275449>.
33. Vairo, C.; Collantes, M.; Quincoces, G.; Villullas, S.; Peñuelas, I.; Pastor, M.; Gil, A.G.; Gainza, E.; Hernandez, R.M.; Igartua, M.; Gainza, G. Preclinical safety of topically administered nanostructured lipid carriers (NLC) for wound healing application: biodistribution and toxicity studies. *Int. J. Pharm.* **2019**, *569*, 118484, <https://doi.org/10.1016/j.ijpharm.2019.118484>.
34. Galvão, J.G.; Santos, R.L.; Silva, A.R.S.T.; Santos, J.S.; Costa, A.M.B.; Chandasana, H.; Andrade-Neto, V.V.; Torres-Santos, E.C.; Lira, A.A.M.; Dolabella, S.; Scher, R.; Kima, P.E.; Derendorf, H.; Nunes, R.S. Carvacrol loaded nanostructured lipid carriers as a promising parenteral formulation for leishmaniasis treatment. *Eur. J. Pharm. Sci.* **2020**, *150*, 105335, <https://doi.org/10.1016/j.ejps.2020.105335>.
35. Ali, R.; Staufenbiel, S. Preparation and characterization of dexamethasone lipid nanoparticles by membrane emulsification technique, use of self-emulsifying lipids as a carrier and stabilizer. *Pharm. Dev. Technol.* **2021**, *26*, 262–268, <https://doi.org/10.1080/10837450.2020.1863427>.
36. López, K.L.; Ravasio, A.; González-Aramundiz, J.V.; Zacconi, F.C. Solid Lipid Nanoparticles (SLN) and Nanostructured Lipid Carriers (NLC) Prepared by Microwave and Ultrasound-Assisted Synthesis: Promising Green Strategies for the Nanoworld. *Pharmaceutics* **2023**, *15*, 1333, <https://doi.org/10.3390/pharmaceutics15051333>.
37. Ghosh Dastidar, D.; Chakrabarti, G. Chapter 6 - Thermoresponsive Drug Delivery Systems, Characterization and Application. In *Applications of Targeted Nano Drugs and Delivery Systems*, Mohapatra, S.S., Ranjan, S., Dasgupta, N., Mishra, R.K., Thomas, S., Eds.; Elsevier, **2019**; 133-155, <https://doi.org/10.1016/B978-0-12-814029-1.00006-5>.
38. Bunjes, H.; Unruh, T. Characterization of lipid nanoparticles by differential scanning calorimetry, X-ray and neutron scattering. *Adv. Drug Deliv. Rev.* **2007**, *59*, 379–402, <https://doi.org/10.1016/j.addr.2007.04.013>.
39. Cova, A.; Müller, A.J.; Laredo, E.; Sandoval, A.J. Effect of two different lipid sources on glass transition temperatures and tensile properties of corn semolina. *J. Food Eng.* **2012**, *113*, 265–274, <https://doi.org/10.1016/j.jfoodeng.2012.05.040>.
40. Abourehab, M.A.S.; Rajendran, R.R.; Singh, A.; Pramanik, S.; Shrivastav, P.; Ansari, M.J.; Manne, R.; Amaral, L.S.; Deepak, A. Alginate as a Promising Biopolymer in Drug Delivery and Wound Healing: A Review of the State-of-the-Art. *Int. J. Mol. Sci.* **2022**, *23*, 9035, <https://doi.org/10.3390/ijms23169035>.
41. Zhang, J.; Fan, Y.; Smith, E. Experimental Design for the Optimization of Lipid Nanoparticles. *J. Pharm. Sci.* **2009**, *98*, 1813-1819, <https://doi.org/10.1002/jps.21549>.
42. Saewan, N.; Jimtaisong, A.; Panyachariwat, N.; Chaiwut, P. In Vitro and In Vivo Anti-Aging Effect of Coffee

- Berry Nanoliposomes. *Molecules* **2023**, *28*, 6830, <https://doi.org/10.3390/molecules28196830>.
43. Asghar, Z.; Jamshaid, T.; Sajid-ur-Rehman, M.; Jamshaid, U.; Gad, H.A. Novel Transethosomal Gel Containing Miconazole Nitrate; Development, Characterization, and Enhanced Antifungal Activity. *Pharmaceutics* **2023**, *15*, 2537, <https://doi.org/10.3390/pharmaceutics15112537>.
44. Shu, X.; Zhang, L.; Liao, W.; Liu, J.; Mao, L.; Yuan, F.; Gao, Y. Nanostructured lipid carriers (NLCs) stabilized by natural or synthetic emulsifiers for lutein delivery: Improved physicochemical stability, antioxidant activity, and bioaccessibility. *Food Chem.* **2023**, *403*, 134465, <https://doi.org/10.1016/j.foodchem.2022.134465>.